Experimental observation of lasing shutdown via asymmetric gain

M. Chitsazi, S. Factor, J. Schindler, H. Ramezani, F. M. Ellis, and T. Kottos
Department of Physics, Wesleyan University, Middletown, Connecticut 06459, USA
(Received 16 July 2013; published 28 April 2014)

Using a pair of coupled RLC cavities we experimentally demonstrate that amplification action can be tamed by a spatially inhomogeneous gain. Under specific conditions we observe the counterintuitive phenomenon of stabilization of the system even when the overall gain provided is increased. This behavior is directly related to lasing shutdown via asymmetric pumping, recently proposed in M. Liertzer *et al.* [Phys. Rev. Lett. **108**, 173901 (2012)]. The analysis of other simple systems reveals the universal nature of the lasing shutdown phenomenon as having its roots in managing impedance matching.

DOI: 10.1103/PhysRevA.89.043842 PACS number(s): 42.55.Ah, 03.65.Nk, 42.25.Bs, 42.55.Sa

I. INTRODUCTION

A laser oscillator consists of a gain medium embedded in an optical cavity. When the pumping level exceeds a threshold value that balances light leakage out of the cavity and other losses, the system self-organizes to emit a narrow-band coherent electromagnetic radiation [1]. Depending on the various geometric characteristics of the confined cavity (chaotic or integrable) [2] and the properties of the index of refraction (uniform, periodic, aperiodic, or random) [3,4] etc., various types of lasing modes have been identified and thoroughly analyzed during the past years. There are also laser systems in which the spatial distribution of the gain medium plays a significant role in determining the properties of the lasing mode [5,6]. Within this framework of spatially inhomogeneous gain, the counterintuitive phenomenon of *lasing death*, i.e., the possibility to shutdown a laser while the overall pump power provided to the system is increased, has been predicted in Ref. [7] based on simulations that make use of a steady-state *ab initio* laser theory [8].

In this paper we establish the applicability of the lasing death (LD) phenomenon beyond the framework of laser physics. We show how it arises in a simple cavity with spatially distributed gain and experimentally demonstrate the lasing death counterpart in its most distilled form consisting of a coupled pair of RLC circuits. A qualitative explanation of lasing death emerges based on fundamental principles of impedance matching within the context of a linear stability analysis of the system.

We remark that LD phenomena have already been reported in the past (see for example [9]); however the underlying mechanism is different. Here, we are concerned with the most fundamental of processes where the LD is not complicated by mode competition. In fact, this is one of the main merits of our RLC analogy as it allows us to experimentally isolate only two lasing modes and investigate, under controlled conditions, their parametric evolution as the overall gain distribution in the setup changes.

The structure of the paper is as follows. In Sec. II we consider the linear lasing behavior of an optical cavity with a simple spatially inhomogeneous gain profile. Using this example, we review the lasing death phenomenon and analyze it using semiclassical laser theory. In the next section, Sec. III, we present our experimental system of two coupled RLC circuits with active nonlinear conductances that determine gain parameters γ_1 and γ_2 and show that for specific pumping paths, the system experiences *two* threshold transitions from nonoscillatory (stable) to self-oscillatory (unstable) dynamics (associated with "lasing action" in the optics framework) despite the fact that the total gain $\gamma = \gamma_1 + \gamma_2$ continually increases along the path [10]. Comparing the two systems, we see that they follow the same passage through lasing death and understand the phenomenon in terms of impedance matching. In Sec. IV we present a universal model which relies on the effective (non-Hermitian) Hamiltonian formalism of scattering that allows us to generalize the LD phenomenon to any system with inhomogeneous gain profile. The formalism explains why a linear stability analysis of an effective non-Hermitian matrix that describes the internal dynamics of an amplifying cavity can be used to successfully predict the occurrences of lasing death. Finally our conclusions are given in Sec. V.

II. INHOMOGENEOUS DISTRIBUTION OF GAIN IN A LASING MICROCAVITY

In order to move consideration of the lasing death phenomenon toward its conceptually simplest manifestation, we first consider a one-dimensional (1D) photonic Fabry-Perot cavity of length $2L$ comprised of two active regions with spatially inhomogeneous gain, shown in Fig. 1(a). In the left region $-L \leqslant z < 0$ the index of refraction is given by $n_1 = n_c - i\gamma_1$ while in the right region $0 < z \leqslant L$ the index profile is given by $n_2 = n_c - i\gamma_2$. The real index of refraction associated with the cavity is n_c, while n_0 [see Fig. 1(a)] is the background index of refraction within which the cavity is embedded. The parameters γ_1, and γ_2 respectively introduce the net gain in the left and right regions via the imaginary part of the index of refraction. Negative values correspond to loss, for example, $\gamma_1 = \gamma_2 = \gamma_0$ with $\gamma_0 < 0$ represents an intrinsic loss common to both cavities. Note that a somewhat different photonic setup was investigated in Ref. [7], using a very sophisticated steady-state *ab initio* laser theory [8]. Here instead we want to show that a simple semiclassical laser theory based on the parametric evolution of the S-matrix poles can be useful in predicting pumping strategies for which lasing death can appear.

We start our analysis by recalling that above the lasing threshold, the system in general has to be treated as nonlinear [8]. At the threshold, however, as long as the field amplitude

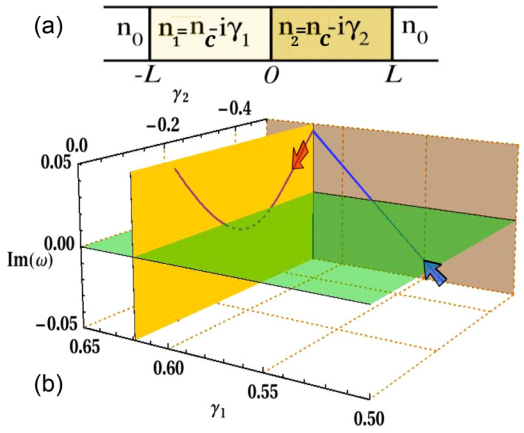

FIG. 1. (Color online) (a) A 1D laser cavity with spatially inhomogeneous gain profile. The cavity occupies the region $-L \leqslant z \leqslant L$. The gain profile is defined by the imaginary part of the index of refraction which take the values $\mathrm{Im}[n_1(-L \leqslant z \leqslant 0)] = -\gamma_1$ and $\mathrm{Im}[n_2(0 \leqslant z \leqslant L)] = -\gamma_2$ where $\gamma_1 \neq \gamma_2$. (b) Parametric evolution of the dominant pole [12] of the scattering matrix S as the gains $\gamma_{1,2}$ change.

is small, it still satisfies the linear Maxwell equations with a negative (amplifying) imaginary part of the refractive index generated by the population inversion associated with a pumping mechanism [1]. Furthermore, it can be rigorously shown within semiclassical laser theory that the first lasing mode in any cavity is an eigenvector of the electromagnetic scattering matrix (S matrix) with an infinite eigenvalue; i.e., lasing occurs when a pole of the S matrix is pulled "up" to the real axis by including gain as a negative imaginary part of the refractive index [11]. We therefore proceed to evaluate the S matrix associated with the structure of Fig. 1(a).

With this configuration, a time-harmonic electric field of frequency ω obeys the Helmholtz equation:

$$\frac{\partial^2 E(z)}{\partial z^2} + \frac{\omega^2}{c^2} n^2(z) E(z) = 0. \tag{1}$$

Equation (1) admits the solution $E_0^-(z) = E_f^- \exp(ikz) + E_b^- \exp(-ikz)$ for $z < -L$ and $E_0^+(z) = E_f^+ \exp(ikz) + E_b^+ \exp(-ikz)$ for $z > L$ where the wave number $k = n_0\omega/c$. The amplitudes of the forward and backward propagating waves outside of the cavity domain are related through the transfer matrix M:

$$\begin{pmatrix} E_f^+ \\ E_b^+ \end{pmatrix} = \begin{pmatrix} M_{11} & M_{12} \\ M_{21} & M_{22} \end{pmatrix} \begin{pmatrix} E_f^- \\ E_b^- \end{pmatrix}. \tag{2}$$

The transfer matrix is evaluated through matrix factors associated with each boundary,

$$M = B\left(\frac{n_2}{n_0}, 1, e^{ikL}\right) B\left(\frac{n_1}{n_0}, \frac{n_2}{n_0}, 1\right) B\left(1, \frac{n_1}{n_0}, e^{-ikL}\right), \tag{3}$$

where $n_1 = n_c - i\gamma_1, n_2 = n_c - i\gamma_2$, and the *algebraic* matrix function $B(\alpha,\beta,u)$ is defined as

$$B(\alpha,\beta,u) = \begin{pmatrix} u^\beta & u^{-\beta} \\ \beta u^\beta & -\beta u^{-\beta} \end{pmatrix}^{-1} \begin{pmatrix} u^\alpha & u^{-\alpha} \\ \alpha u^\alpha & -\alpha u^{-\alpha} \end{pmatrix}. \tag{4}$$

In this function, α and β are the relative index of refraction steps on the left and right side of a boundary at a position defined by u, and, due to the complex nature of α and β, a numerical evaluation of M requires the algebraic substitution of the parameters of Eq. (3) into Eq. (4) to assure evaluation of the appropriate Riemann sheet.

The transmission and reflection amplitudes for left (L) and right (R) incidence waves are obtained from the boundary conditions $E_b{}^+ = 0$, and $E_f{}^- = 0$ respectively, and are defined as $t_L \equiv \frac{E_f{}^+}{E_f{}^-}$, $r_L \equiv \frac{E_b{}^-}{E_f{}^-}$; and $t_R \equiv \frac{E_b{}^-}{E_b{}^+}$, and $r_R \equiv \frac{E_f{}^+}{E_b{}^+}$. These are expressed in terms of the M-matrix elements:

$$t_L = t_R = t = \frac{1}{M_{22}}; \quad r_L = -\frac{M_{21}}{M_{22}}; \quad r_R = \frac{M_{12}}{M_{22}}. \tag{5}$$

From these relations we evaluate the S matrix as

$$\begin{pmatrix} E_f^+ \\ E_b^- \end{pmatrix} = S \begin{pmatrix} E_b^+ \\ E_f^- \end{pmatrix}; \quad S = \begin{pmatrix} r_L & t \\ t & r_R \end{pmatrix}, \tag{6}$$

which below the first lasing threshold, connects the outgoing wave amplitudes to their incoming counterparts.

Scattering resonances correspond to purely outgoing boundary conditions on the S matrix, i.e., $(E_f{}^+, E_b{}^-)^T \neq 0$ while $(E_b{}^+, E_f{}^-)^T = 0$, and occur when the S matrix has a pole in the complex plane. It follows from Eqs. (5) and (6) that the poles $\omega_p = \omega_R - i\omega_I$ of the S matrix can be identified with the complex zeros of the characteristic equation $M_{22} = 0$. As pointed out in Ref. [13], the poles of the S matrix that lay on the real axis are associated with physically meaningful states which are termed "threshold lasing modes."

In Fig. 1(b) we report the evolution of $\mathrm{Im}(\omega)$ for the dominant pole of the S matrix for a specific path of the gain parameters γ_1, γ_2 associated with the left and right portions of the cavity. The dominant pole is the only one to experience the stability-instability transitions within the frequency range assumed for the γ_1 and γ_2 gain curves [12]. Initially, we assume that both the left and right regions of the optical cavity have the same intrinsic loss $\gamma_0 < 0$ as described earlier. The left part of the cavity is then pumped with increasing gain, $\gamma_0 < \gamma_1 < \gamma_1^{\max}$, until the dominant pole crosses the real axis [$\mathrm{Im}(\omega) = 0$] at some critical gain $\gamma_1^* < \gamma_1^{\max}$. At this point, a lasing state in the cavity is created. For $\gamma_1^* < \gamma_1 < \gamma_1^{\max}$ the pole continues to travel upwards in the positive [$\mathrm{Im}(\omega) > 0$] plane indicating unstable dynamics. In this regime, any physical system ultimately becomes nonlinear and the scattering approach fails. However, we may infer from our low amplitude linear analysis the presence or absence of the lasing instability. The pumping on the left partition is now kept constant at $\gamma_1 = \gamma_1^{\max}$, while additional pumping, via increasing γ_2, is applied to the right partition of the cavity. Surprisingly, this results in reversing the evolution of the pole back towards $\mathrm{Im}(\omega) = 0$. At some critical value $\gamma_2 = \gamma_2^*$, the pole recrosses the real axis returning to $\mathrm{Im}(\omega) < 0$. Such transitions indicate that the system returns to stability, i.e., the laser shuts off despite the fact that the overall pump power provided to the system has been increased. Further increase of γ_2 once again reverses the direction of the motion of the pole which moves upwards and crosses into $\mathrm{Im}(\omega) > 0$. At this new critical value, $\gamma = \gamma_2^{**}$, the mode once again becomes unstable signifying a second turn-on of the laser.

Finally, it is instructive to point out that it is possible to express the S matrix at an arbitrary wave number k in terms of all eigenvalues and eigenfunctions of the corresponding closed cavity. This is achieved by employing the so-called reaction matrix formalism which has been developed in the frame of nuclear physics by Wigner and Eisenbud [14]. Specifically we have that

$$S = \frac{\hat{1} - iK}{\hat{1} + iK}; \quad K = \pi W^{\dagger} G_{\rm in} W, \tag{7}$$

where K is the so-called reaction matrix and $(G_{\rm in})_{n,n'} = [k^2(\delta_{n,n'} - i\hat{\Gamma}_{n,n'}) - k_n^2\delta_{n,n'}]^{-1}$ is the Green's function of the closed active cavity. The gain matrix $\hat{\Gamma}$ denotes the gain distribution inside the cavity and the matrix $\hat{W}(k)$ denotes the coupling of the internal level n to the scattering channel j. Equation (7) can be further expressed [15] in terms of an effective non-Hermitian Hamiltonian $\mathcal{H}_{\rm eff}$ which contains the dynamics of the closed system and the coupling to the scattering channels:

$$S = \hat{1} - 2i\pi W^{\dagger} G_{\rm eff} W; \quad G_{\rm eff} = [\mathcal{E} - H_{\rm eff}]^{-1}, \tag{8}$$

where $(\mathcal{H}_{\rm eff})_{n,n'} = k_n^2\delta_{n,n'} - i\pi(WW^{\dagger})_{n,n'}$ and $\mathcal{E} = k^2(\hat{1} - \hat{\Gamma})$. We see therefore that the poles of the scattering matrix are the complex eigenvalues of an effective Hamiltonian. Although we will make use of the effective Hamiltonian formalism only in Sec. IV, it is useful at this point to keep in mind the equivalence between the various forms of the scattering matrix.

III. LASING DEATH FOR COUPLED *RLC* CIRCUITS

We now simplify the previous concept to its essence and experimentally demonstrate the universality of the lasing death phenomenon. To this end we have distilled the trade-off of gain and loss responsible for lasing into its fundamental form, gain (or loss) in a simple oscillator. We further include the spatially distributed gain required for lasing death by considering a coupled *pair* of oscillators, each with their own gain (or loss). Figure 2 schematically illustrates the experimental circuit. Conductances of either sign placed in parallel with each

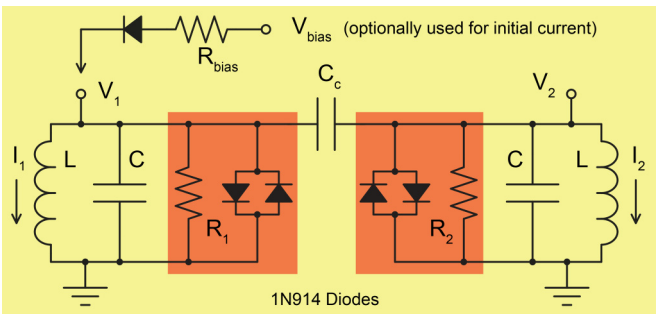

FIG. 2. (Color online) A pair of coupled LC resonators with parallel conductances (shaded) and coupling capacitance C_c. The conductance of each LC unit is equivalent to resistances R_1 and R_2 which can be of either sign, providing gain if negative, or loss if positive. The back-to-back diodes impose a lossy nonlinear contribution to conductance to assure a well-behaved limit cycle in the self-oscillatory (unstable) regime. An initial current can be injected using the bias circuit at the top.

LC resonator provide the gain parameters $\gamma_1 = -\frac{1}{R_1}\sqrt{\frac{L}{C}}$ and $\gamma_2 = -\frac{1}{R_2}\sqrt{\frac{L}{C}}$. The coupled resonator circuit is similar to that used previously [16] where the active conductance of each LC unit is implemented with a parallel combination of a positive resistance with a variable negative resistance provided by a negative impedance converter. This combination allows control of the total conductance over both positive and negative values, and thus exploration of the gain parameter space (γ_1, γ_2) in all quadrants. We consider only capacitive coupling between the oscillator pair, and restrict the discussion to matched LC resonators.

In order to make contact with saturable laser dynamics and ensure graceful behavior above threshold, a simple conductance nonlinearity is included by the addition of back-to-back 1N914 diodes, also in parallel with the LC resonators, as shown. This forces a dominant positive conductance (loss) at high voltage amplitudes, and assures a well behaved limit cycle when the system is unstable, above any oscillation threshold. The linear regime is below approximately 150 mV, where the diodes have negligible conductance.

Application of the first and second Kirchhoffs laws [17] leads to the following set of equations for the LC node voltages V_n and inductor currents I_n, shown in the schematic of Fig. 2:

$$V_n = L\dot{I}_n$$
$$\frac{V_n}{R_n} + I_{\rm sat}\sinh\left(\frac{V_n}{V_t}\right) + C\dot{V}_n + I_n + C_c(\dot{V}_n - \dot{V}_{3-n}) = 0. \tag{9}$$

In our experimental circuit, $L = 10\ \mu$H and $C = 328$ pF as measured by the uncoupled frequencies $\omega/2\pi = 2.78$ MHz after trimming the LC resonators to within 1% of each other. The coupling capacitance is $C_c = 56$ pF. The parameters $I_{\rm sat} = 4.0$ nA and $V_t = 47$ mV are the reverse bias saturation current and the thermal voltage in the Shockley ideal diode equation [18]. We note that the RLC pair can alternatively be considered as coupled to output leads connected to the LC nodes if the resistances R_1 and R_2 are re-interpreted as including the parallel characteristic impedance Z_0 of TEM transmission line leads. With Z_0 real and frequency independent, as is the case for TEM transmission lines, nonzero voltage V_1 or V_2 are then interpreted as coupling power into the corresponding transmission line—the analog of radiated optical power in a laser.

A. Dynamics and stability analysis of the *RLC* circuit

The LD behavior for our electronic circuit can be experimentally confirmed via steady-state measurements of the RMS voltage $V_{\rm rms}$ of either node as we increase the overall gain of the system. In a close analog to a laser [7], our system is considered stable when $V_{\rm rms} = 0$. In contrast when the system is unstable, a nonzero value of $V_{\rm rms}$ is measured that is dictated by the circuit saturation dynamics, in this case the back-to-back signal diodes. Mathematically, the saturation dynamics is determined by the nonlinear $\sinh(\cdots)$ term in the second Eq. (9).

The data in Fig. 3 correspond to several paths of increasing γ_2, along the vertical lines shown in the inset, with $\gamma_1 = $ const.

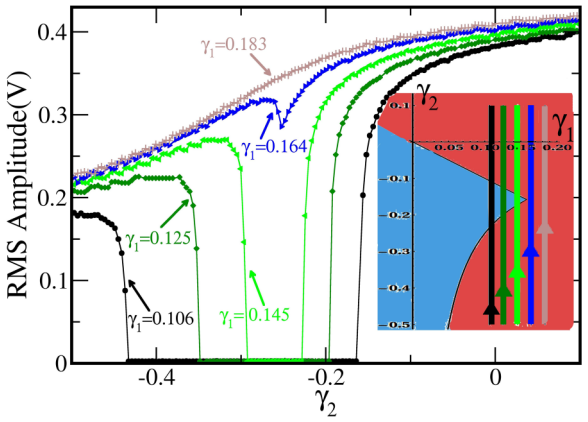

FIG. 3. (Color online) Experimental steady-state voltage for paths of increasing γ_2 at fixed γ_1 shown in the inset. The voltage was measured on the side-1 LC node. Note that the width of the "lasing death" response diminishes as the overall gain increases.

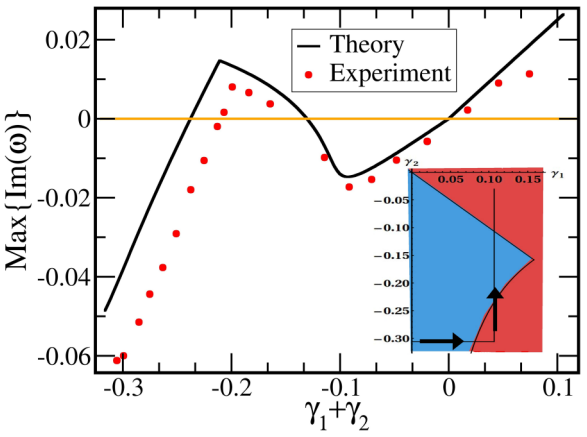

FIG. 4. (Color online) The theoretical and experimental maximum imaginary part of all eigenfrequencies is shown as total gain (horizontal axis) is increased. The pumping path is illustrated by the stability diagram (inset). The "lasing death" phenomenon occurs when the path traverses a protrusion in the stability map—the most positive imaginary part momentarily dips back into the negative region. The vertical path in the inset corresponds to the black curve of Fig. 3 where the steady-state saturation amplitude was presented.

In all cases the total gain $\gamma_1 + \gamma_2$ provided to the system is increased. We find that depending on the value of γ_1 the system either undergoes a transition from instability to stability or it remains unstable all the time. The former case corresponds to the phenomenon of lasing death found numerically in Ref. [7] or in the simplified model of Sec. II and is achieved only for the leftmost three pumping paths shown in the inset of Fig. 3.

Next we want to understand which pumping paths can result in lasing death. As in the last section, we argue that these paths are associated with the existence of reentrant stability domains in the (γ_1,γ_2) plane which are traversed by the specific pumping schemes. In this respect, every time that a path crosses a boundary between an unstable to stable domain we have a suppression of lasing action and thus the emergence of lasing death.

To substantiate this assertion, we again analyze the linearized equations associated with our system Eq. (9). Note that the linear equations of motion, with the sinh term omitted [19], will describe the dynamics of our system provided all voltages and currents remain below any nonlinearities of the actual circuit—approximately 150 mV in the case of our circuit.

Substituting the optical convention time periodic solution $(V_n, I_n)^T = \exp(-i\omega' t)(V_n^0, I_n^0)^T$ and eliminating the I_n^0 we get the following homogeneous equation:

$$\begin{pmatrix} \frac{1}{\omega} - \omega(1+c) - i\gamma_1 & \omega c \\ \omega c & \frac{1}{\omega} - \omega(1+c) - i\gamma_2 \end{pmatrix} \begin{pmatrix} V_1 \\ V_2 \end{pmatrix} = 0, \tag{10}$$

where the parameters $\omega = \omega'\sqrt{LC}$ and $c = C_c/C$ are a scaled frequency and coupling strength, and the γ_1 and γ_2 are the gain parameters previously defined. The eigenfrequencies are found by setting the determinant of the coefficient matrix in Eq. (10) equal to zero, and solving the characteristic polynomial.

The imaginary part of the eigenfrequencies ω of the system Eq. (10) dictate the stability of the system: the circuit is unstable if any of the modes have a positive imaginary part, otherwise it is stable. For a stable circuit all transient solutions are decaying, while for the unstable circuit, there is at least one exponentially growing solution corresponding to the electronic analog of "lasing" into the effective transmission lines.

The shaded domains in the inset of Fig. 3 map the system stability in the gain parameter space with the unstable domain extending into the regions of large positive γ_n. The pumping path associated with the top data set corresponds to large enough γ_1 to completely miss the stable region as γ_2 is increased. Subsequent paths along increasing γ_2 with smaller values of γ_1 pass progressively deeper through the reentrant stability region, resulting in complete extinction of the oscillation followed by a new threshold. The data sets illustrate how the linear stability map is directly related to the observed reentrant stability response of the nonlinear system. In a real laser system with a more complex saturation dynamics, hysteresis will likely distort this correspondence, but the position of a second threshold in a restabilized state will always be determined by the linearized behavior.

Figure 4 shows the evolution of experimental values for $\mathrm{Im}(\omega)$ as a function of total gain, defined as $\gamma_1 + \gamma_2$ obtained along the path in the (γ_1,γ_2) stability map shown in the inset. The color scheme used is the same as that of Fig. 3. Experimental frequencies are obtained by imposing an initial dc current in side $n = 1$ through a forward biased 1N914 signal diode. The bias voltage of the optional injection circuit of Fig. 2 is then rapidly switched to a reverse-biased state, where the contribution to the circuit is the small $\approx$0.3 pF junction capacitance of the reverse biased diode. The subsequent voltage evolution on node $n = 1$ is recorded and fit to a generic double-resonance transient to obtain the complex eigenfrequencies, from which the mode with the most positive imaginary part is identified.

Let us now compare the experimental stability diagram of Fig. 4 with the experimental measured temporal dynamics of the RLC circuit shown in Fig. 3. Starting along the horizontal path of Fig. 4 (inset), the "lasing action" of our electronic system turns on at a first threshold of stability as γ_1 is increased

for fixed γ_2 (correlate this path with the data shown with a black line in Fig. 3) rising up through $\mathrm{Im}(\omega) = 0$. Continuing along the vertical path in the inset, as γ_2 is increased with γ_1 fixed, the lasing death (amplification death) is realized as the path cuts through the protruding section of the stability map. Along this path, the imaginary part of the eigenfrequency drops back into the stable regime with $\mathrm{Im}(\omega) < 0$, then turns around and finally becomes permanently positive (unstable). Note that the complete path follows one of monotonically increasing total gain and experiences both turn-on thresholds.

Finally we have confirmed that, in the scattering configuration with TEM transmission lines of impedance Z_0 attached to the LC nodes, the eigenfrequencies of the linear Eq. (10) are identical to the poles of the circuit Smatrix with the gain parameters γ_1 and γ_2 reduced by $\Delta\gamma = \frac{1}{Z_0}\sqrt{\frac{L}{C}}$, the transmission line contact loss. We used the mathematical framework of scattering in Sec. II and will make use of this formulation in Sec. IV where we discuss a universal description of the LD phenomenon in terms of the movement of the poles of the scattering matrix associated with the system in question.

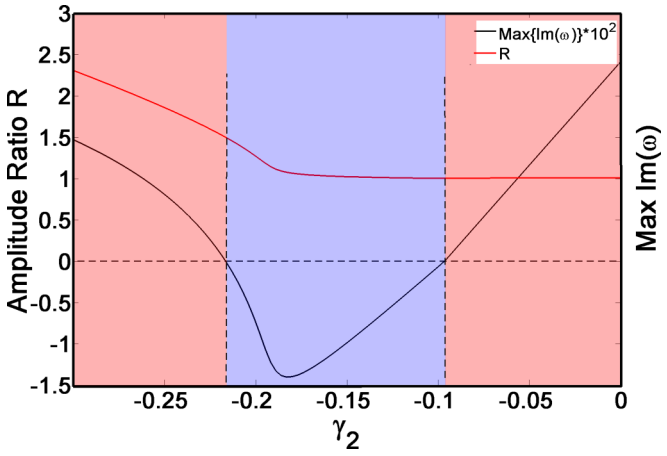

FIG. 5. (Color online) The parametric evolution of the ratio $\mathcal{R}$ between the two components of the most unstable linear mode (red line). For comparison we also report the Max $\mathrm{Im}(\omega)$. Three domains are identified: The most left and the right domains are associated to $\mathcal{R} > 1$ and $\mathcal{R} = 1$ and correspond to unstable dynamics. The middle domain is associated with the LD phenomenon and it indicates stable dynamics.

B. Normal-mode analysis and impedance mismatching as the origin of Lasing death

Although Eqs. (9) that describe the dynamics of the two coupled RLC oscillators are intrinsically nonlinear it is nevertheless instructive to analyze the structure of the normal modes $(V_1^{(i)}, V_2^{(i)})^T$ of the linearized relations Eq. (10) of the RLC circuit pair along a pumping path exhibiting the LD phenomenon. Our investigation will focus on the most unstable normal mode, calculated via Eq. (10) after substituting for ω the frequency which corresponds to the Max[$\mathrm{Im}(\omega)$]. We will indicate this frequency below with the superindex 1, e.g., $\omega^{(1)}$ and the corresponding normal-mode components as $(V_1^{(1)}, V_2^{(1)})^T$.

It is at this juncture that the simplicity of the electronic circuit proves insightful. If the RLC nodes are considered as connected to transmission lines—with appropriate reinterpretation of the gain or loss parameters γ_1 and γ_2 to including the corresponding output-coupling loss—the voltage amplitudes V_1 and V_2 serve as direct indicators of *all* of the quantities of interest: (1) the character of the normal mode through the relative amplitudes of the left and right RLC oscillations; (2) the output power $\frac{1}{2}|V_n|^2/Z_0$ coupled into the transmission lines; and (3) the input power $\frac{1}{2}|V_n|^2(\gamma_n - 1/Z_0)$ supplied by the pumping sources associated with each node.

The details of the lasing death are then revealed through Fig. 5 where we show $\omega^{(1)}$ as well as the ratio $\mathcal{R} = |V_1^{(1)}/V_2^{(1)}|$ along the reentrant portion of Fig. 4, as a function of γ_2 with $\gamma_1 = 0.0967$ fixed. Starting from the left with large negative values of γ_2, we find the system in the unstable regime. How is this possible with negative total gain $\gamma_1 + \gamma_2$? The value of $\mathcal{R}$ indicates that the normal mode is dominated by oscillations of the node with the positive gain. The mode configuration thus "spatially overlaps" the gain. Why then does the lasing death happen in spite of the total gain being increased? As γ_2 increases, the mode shifts toward a balanced configuration with $\mathcal{R} \sim 1$, exposing the system to a total accepted input power more closely reflecting the *still negative* total gain $\gamma_1 + \gamma_2$. Finally, as γ_2 continues to increase, with $\mathcal{R} \sim 1$ confirming that the balanced mode configuration persists, the total input power once again overcomes the losses (including the output coupling) and the system crosses back above threshold.

Within the context of resonant structure electronics, the alignment of the normal modes relative to a particular circuit node defines that node's impedance. We can thus interpret the lasing death phenomenon as an impedance matching transition mediated by the gain dependent reconfiguration of the normal modes. This type of dramatic reconfiguration can only occur concurrent with spatially distributed gain, and is associated with, though not necessarily close to, exceptional points of the system [16].

The similarities of "stabilization induced via gain" between the electronics and optics systems indicate that the underlying physical mechanism in these seemingly unrelated systems is the same. The following heuristic argument provides some qualitative understanding of the LD phenomenon in the frame of optical cavities. Referring back to the 1D laser cavity of Fig. 1, when the pumping on the left partition has reached its maximum value the impedance mismatch between the two partitions is maximal. As a result the two parts of the photonic cavity are effectively decoupled and the photons are trapped only on the left partition where they experience maximal gain. At this point the outgoing field intensity reaches its maximum value and is associated with emission from the left (gain) partition (see the numerical simulations of Ref. [7]). An increase of the gain in the right partition of the cavity, while keeping a constant pumping rate on the left, leads to "softening" of the impedance mismatch between the two domains. As a result, photons start exploiting the right domain. However, as they dwell in the right portion of the cavity, they are experiencing less gain (with respect to the previous case when they were confined to the high-gain side due to impedance mismatch). As a result the outgoing field intensity

is weakened and becomes more uniform (still though, it is dominated by an outgoing field coming from the left side). At this point, depending on the pumping path, two scenarios can be found: (a) If the maximum gain of the left partition is well above the lasing threshold, the cavity will remain unstable and the impedance matching process will result only in decreasing the outgoing intensity. The second scenario corresponds to a "marginal" lasing threshold due to the pumping of the left partition. In this case, a reduction of the impedance mismatch will lead to further suppression of the total gain that a photon will accumulate as it explores the total cavity. Such a process leads to stabilization of the laser cavity and the appearance of the lasing death phenomenon. When the gain in the right partition exceeds a critical value the photons experience strong amplification irrespective of their position inside the cavity. At this point the cavity again reaches a lasing threshold with a symmetric outgoing field intensity.

IV. EFFECTIVE NON-HERMITIAN HAMILTONIAN FORMALISM

The universality of lasing death via asymmetric pumping can also be illustrated within a simple two-level model (dimer) coupled to two leads. The system is shown in the inset of Fig. 6. The Hamiltonians of the dimer H_d and of the leads H_{leads} read

$$\begin{aligned} H_d &= \sum_{n_N=1,2} \epsilon_{n_N} |n_N\rangle\langle n_N| + (|n_N\rangle\langle n_N+1| + \text{c.c.}), \\ H^{L,R}_{\text{leads}} &= \sum_{n=n_L,n_R} \epsilon_n |n\rangle\langle n| + (|n\rangle\langle n+1| + \text{c.c.}), \end{aligned} \tag{11}$$

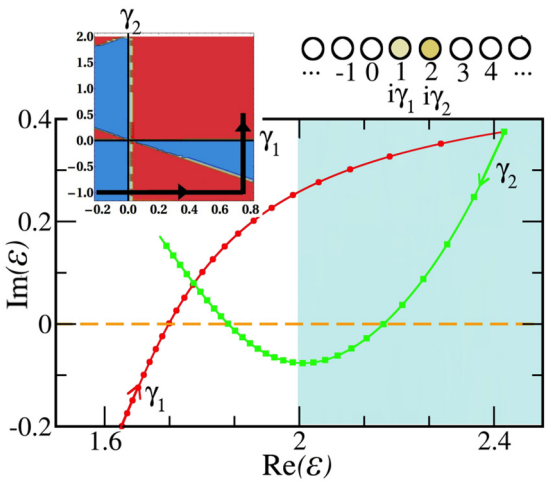

FIG. 6. (Color online) Right inset: A simple tight-binding model consisting of two active discrete elements coupled to two semi-infinite left and right leads. Left inset: The stability phase diagram of the TB system. Red areas indicate unstable $\gamma_1 - \gamma_2$ domains while blue areas indicate stable domains. The arrows indicate the direction of the pumping path. Main panel: Parametric evolution of one of the two resonances as the pumping γ_1 at site $n_N = 1$ and γ_2 at site $n_N = 2$ changes. The arrows indicate the evolution of resonances as γ_1,γ_2 increases. The parametric evolution of the second resonance is not shown since its motion is symmetric to the one reported here with respect to the origin of the axis $\text{Re}(\mathcal{E})$.

where $n_L = 0,\ldots,-\infty$, $n_R = 3,\ldots,\infty$, and $\{|n\rangle\}$ is the Wannier basis of the tight-binding Hamiltonian. The on-site potentials are $\epsilon_n = V_n + i\gamma_n$ with $\gamma_n = 0$, for $n \neq 1,2$ [20]. Furthermore, without loss of generality we will assume that $V_n = 0$ for all n. The complex zeros $\mathcal{E}$ of the secular equation $\det[M_{22}(\mathcal{E})] = 0$ can be calculated analytically:

$$\mathcal{E} = \frac{i[\gamma_1\gamma_2(\gamma_1+\gamma_2) \pm (2+\gamma_1\gamma_2)\sqrt{(\gamma_1-\gamma_2)^2-4}]}{2(1+\gamma_1\gamma_2)}. \tag{12}$$

In Fig. 6 we present a parametric evolution of the poles $\mathcal{E}$ for a pumping path (see left inset) analogous to the previous discussion: an initial increase of γ_1 until the lasing threshold is reached, followed by an increase of γ_2. As before, during the second section of the path the system is first driven back towards stability (lasing death) while later on it returns to instability at a second lasing threshold. We note that the pumping path within the shaded region of Fig. 6 has to be excluded from our analysis. Here, the poles have $\text{Re}(\mathcal{E}) > 2$ and the scattering modes fall outside of the propagation band $E(k) = 2\cos(k)$ of the leads.

The generality of the lasing death phenomenon calls for a universal formulation for its explanation. Using standard methods [21] we write the scattering matrix elements in the form [22,23]

$$S_{\alpha,\beta}(E) = \delta_{\alpha,\beta} - i\sqrt{4-E^2}\,\mathcal{W}^T_\alpha (E - \mathcal{H}_{\text{eff}})^{-1}\mathcal{W}_\beta, \tag{13}$$

where $\alpha,\beta = 1,2$ and $\mathcal{H}_{\text{eff}}$ is a 2×2 effective non-Hermitian Hamiltonian given by

$$\mathcal{H}_{\text{eff}}(E) = H_d + \Sigma(E)\sum_\alpha \mathcal{W}_\alpha \bigotimes \mathcal{W}^T_\alpha. \tag{14}$$

The two-dimensional vectors $\mathcal{W}_1 = \delta_{\alpha,1}$ and $\mathcal{W}_2 = \delta_{\alpha,2}$ describe at which site we couple the leads with our sample while $\Sigma(E) = \frac{E - i\sqrt{4-E^2}}{2}$ is the so-called self-energy.

The poles of the S matrix are equal to the complex zeros $\mathcal{E}$ of the following secular equation:

$$\det[\mathcal{E} - H_{\text{eff}}(\mathcal{E})] = 0. \tag{15}$$

Solving Eq. (15) is (in general) a difficult task. However, there are circumstances such as the RLC circuit previously discussed, for which one can neglect the dependence of H_{eff} on energy. In such cases the second term in Eq. (14) results in a simple constant shift of the on-site potential of the Hamiltonian H_d.

From the above discussion we conclude that the stability of our system and the lasing death phenomenon are directly linked with the stability diagram and the parametric evolution of the complex eigenvalues $\mathcal{E}$ of H_{eff}. Specifically the sign of their imaginary part $\text{Im}(\mathcal{E})$ defines the stability $[\text{Im}(\mathcal{E}) < 0]$ or instability $[\text{Im}(\mathcal{E}) > 0]$ of the associated modes and therefore of the system itself. For example for the system of Eq. (11) we find that the corresponding eigenvalues of H_{eff} are given by Eq. (12). We include the associated stability diagram in the left inset of Fig. 6. As before, unstable domains are indicated with red and are associated with an imaginary part of one of the eigenvalues being larger than zero. The stable domains are indicated with blue and they correspond to gain parameters γ_1,γ_2 for which $\text{Im}(\mathcal{E}) < 0$. It is therefore obvious that one can select pumping paths in the (γ_1,γ_2) plane which lead to

transitions from stability to instability and back to stability while $\gamma_1 + \gamma_2$ is continuously increasing through the pumping process.

V. CONCLUSIONS

To summarize, we have identified a generic link between spatially distributed gain and the phenomenon of lasing death, and experimentally demonstrated the phenomenon in a simple coupled LC oscillator system. We have analyzed the phenomenon in several model systems, including the coupled RLC pair. We have shown how and why the output can be extinguished over an interval of increasing system gain. This unorthodox and robust effect of restabilization via gain is universal with roots in a gain-induced change in impedance matching which can lead to a reentrant structure in the stability phase diagram. Only nonuniformly active systems can exhibit this behavior.

Note added in proof. Recently, we became aware of a photonics experimental realization of the lasing death phenomenon [24].

ACKNOWLEDGMENTS

This research was supported by AFOSR MURI Grant No. FA9550-14-1-0037, and by NSF Grant No. ECCS-1128571. S.F. acknowledges support from Wesleyan Faculty-Student Internship grants. Useful discussions with Dr. L. Ge are greatly appreciated.

[1] H. Haken, *Laser Light Dynamics* (North-Holland, Amsterdam, 1986).

[2] A. D. Stone, Nature (London) **465**, 696 (2010); H. G. L. Schwefel, H. E. Tureci, A. Douglas Stone, and R. K. Chang, in *Optical Microcavities* (World Scientific, Singapore, 2005), p. 415; J. U. Nöckel and A. D. Stone, Nature (London) **385**, 45 (1997).

[3] L. Dal Negro and S. V. Boriskina, Laser Photon. Rev. **6**, 178 (2012).

[4] H. Cao, J. Phys. A: Math. Gen. **38**, 10497 (2005).

[5] G. H. B. Thompson, *Physics of Semiconductor Laser Devices* (Wiley & Sons, New York, 1980), Chap. 6.

[6] H. Kogelnik and C. V. Shank, J. Appl. Phys. **43**, 2327 (1972); Y. Luo, Y. Nakano, and K. Tada, Appl. Phys. Lett. **56**, 1620 (1990).

[7] M. Liertzer, Li Ge, A. Cerjan, A. D. Stone, H. E. Türeci, and S. Rotter, Phys. Rev. Lett. **108**, 173901 (2012).

[8] H. E. Türeci, A. D. Stone, L. Ge, S. Rotter, and R. J. Tandy, Nonlinearity **22**, C1 (2009).

[9] J. Andreasen and H. Cao, Opt. Lett. **34**, 3586 (2009).

[10] We clarify that our notion of "total gain increase" also includes the scenario where the loss in the system is reduced. Such an operation leads obviously to a net increase in overall gain. In this respect the connection between our gain parameter γ and the pumping parameter d_{pump} used in Ref. [7] is $\gamma = d_{\text{pump}} + d_{\text{open}}$, where d_{open} is due to the radiated losses from the cavity due to the fact that it is open. In our system d_{open} is fixed and is associated with the inherent losses of the circuit. Therefore when γ increases this signifies that a d_{pump} term is added (i.e., gain in included).

[11] K. M. Frahm *et al.*, Europhys. Lett. **49**, 48 (2000).

[12] We have limited the frequency dependence of the gain profiles to exclude gain for all higher frequency poles than that shown in the figure. Furthermore we have checked numerically that all lower poles remain stable and are not presented in Fig. 1.

[13] L. Ge, Y. D. Chong, S. Rotter, H. E. Türeci, and A. D. Stone, Phys. Rev. A **84**, 023820 (2011).

[14] E. P. Wigner and L. Eisenbud, Phys. Rev. **72**, 606 (1946).

[15] Y. Fyodorov and H.-J. Sommers, J. Math. Phys. **38**, 1918 (1997); P. Mello, *Chaos and Quantum Physics* (Les Houches Summer School), edited by E. Akkermans, G. Montambaux, J. L. Pichard, and J. Zinn-Justin (North-Holland, Amsterdam, 1994), pp. 437–491.

[16] J. Schindler, Z. Lin, J. M. Lee, H. Ramezani, F. M. Ellis, and T. Kottos, J. Phys. A: Math. Theor. **45**, 444029 (2012).

[17] P. Horowitz and W. Hill, *The Art of Electronics* (Cambridge University Press, New York, 1989), Chap. 1.

[18] C. Kittel, *Introduction to Solid State Physics* (John Wiley & Sons, New York, 1996), p. 572.

[19] The linearized sinh term has a negligible conductance contribution $I_{\text{sat}}/V_t = 85$ nS that can be accommodated into $1/R_n$.

[20] Unlike the optical cavity, $\text{Im}(\epsilon_n) > 0$ represents gain while $\text{Im}(\epsilon_n) < 0$ represents loss.

[21] C. Mahaux and H. A. Weidenmüller, *Shell Model Approach in Nuclear Reactions* (North-Holland, Amsterdam, 1969); I. Rotter, Rep. Prog. Phys. **54**, 635 (1991).

[22] J. A. Mendez-Bermudez and T. Kottos, Phys. Rev. B **72**, 064108 (2005).

[23] T. Kottos and M. Weiss, Phys. Rev. Lett. **89**, 056401 (2002).

[24] M. Brandstetter, M. Liertzer, C. Deutsch, P. Klang, J. Schöberl, H. E. Türeci, G. Strasser, K. Unterrainer, and S. Rotter, arXiv:1404.1837.